自然災害科学 *J. JSNDS 36* 特別号 *123-137* (*2017*)

DYNAMICS OF SAND BARS IN A BRAIDED RIVER: A CASE STUDY OF BRAHMAPUTRA-JAMUNA RIVER

SHAMPA[1], Yuji HASEGAWA[2], Hajime NAKAGAWA[2], Hiroshi TAKEBAYASHI[2] and Kenji KAWAIKE[2]

DYNAMICS OF SAND BARS IN A BRAIDED RIVER:
A CASE STUDY OF BRAHMAPUTRA-JAMUNA RIVER

Shampa[1], Yuji Hasegawa[2], Hajime Nakagawa[2],
Hiroshi Takebayashi[2] and Kenji Kawaike[2]

Abstract

Simultaneous reworking with numerous channels and bars makes a dynamic braiding network. In this study, we investigated the response of a braided river planform due to unsteady flow, focusing on the dynamics of bars using a numerical simulation tool in a reach of Brahmaputra-Jamuna River with dominant compound bars. The results indicate that the frequency of deposition on the river bed or a braided plain was higher compared to erosion within the study reach due to unsteady changes of the flow boundary conditions. The results also indicate that the development processes of braided bars are quite different from bars of straight and meandering channels. The spatial growth of the bars seems to be dependent on the width-depth ratio of the river up to a certain range and the migration rate of the bars recedes with the spatial growth of the bars.

Key words：Braided River, Brahmaputra-Jamuna, Bar dynamics, Numerical model, Delft3D.

1. INTRODUCTION

Characterized by numerous transient mid-channel bars and channels, braided rivers possess fascinating, distinctive planforms. The planform changes rapidly and unpredictably in the case of a sand bed due to the relatively high energy and intense bedload transport condition, which accelerates instability especially for mid-channel bars (Ashmore, 2013; Egozi et al., 2009). These bars show various planforms, which seem to be stage-dependent and eventually construct a very wide range of alluvial planforms due to upstream

[1] Department of Civil and Earth Resources Engineering, Kyoto University, Japan

[2] Disaster Prevention Research Institute, Kyoto University, Japan

and downstream erosion and sedimentation (Bridge, 1993; Ashworth et al., 2011). Therefore, in the case of a highly sediment-laden, sand-bed braided river, different types of bars are found such as unit bars and compound bars (in accordance with formation) as well as free bars (mid-channel bars) and force bars (based on forcing) (Schuurman et al., 2013).

The linear bar theory clarifies the relationship between the bar dimensions and the geometry of the channel, which has also been verified by many laboratory experiments, field observations, and mathematical analyses (Muramoto and Fujita, 1978; Colombini et al., 1987; Ikeda, 1990; Yalin, 1992; Garcia and Nino, 1993; Schuurman et al., 2013) but in the case of a highly-sediment-laden braided river that contains many compound bars, the theory may not always apply. Nevertheless, linear bar theory simplifies some nonlinear physical processes that dominate fully developed bars in a braided river. Moreover, the interaction of compound bars and unit bars with a braided plain is poorly understood (Kleinhans and van den Berg, 2011; Schuurman et al., 2013). Some researchers (Sarker et al., 2003; ISPAN, 1993) used satellite imagery analysis to understand this type of interaction but the relation between the river hydraulics and the bar dynamics needs clarifying, and in this case, two-dimensional numerical simulations can be used to understand the river behavior. Hence, in this study, we examined the response of a braided planform due to the change of the flow hydrograph from the start of the wet period to the peak flow of the wet period, focusing on the bar properties of a highly-sediment-laden, sand-bed braided river.

The main objective of this study was to assess the morphological changes of the river, especially the response of braided bars during unsteady flow changes (flow changes in the monsoon season). The relationship of the geometrical properties of the bar and channel during the peak flow was examined. Attention was also given to the migration process of the sand bars. A 225-km reach of Brahmaputra- Jamuna (downstream continuation of the Brahmaputra River in Bangladesh, see **Fig. 1**) was selected as the study site. The river is extremely dynamic, with a high sediment transport rate (Baki and Gan, 2012; Sarker et al., 2014). The morphological features of the river (bars and channels) experience major changes in area, shape and spatial distribution each year in response to the pulsation of discharge and sediment load during periods of flooding (the annual fluctuation of discharge is more than 60,000 m^3/s) (Sarker et al., 2014).

2. METHODOLOGY

2. 1 GENERAL APPROACH

As mentioned earlier, according to the process of development, the bars of Brahmaputra-Jamuna can be divided into two categories, compound bars (A) and unit bars (B) as shown in **Fig. 2**. Similar to sand-bed braided rivers, compound bars are more frequent in this reach compared to unit bars. Although most of these compound and unit bars are free mid-channel bars, some force bars are also found (as shown by C in **Fig. 2**). The growth of unit bars is comparatively straightforward com-

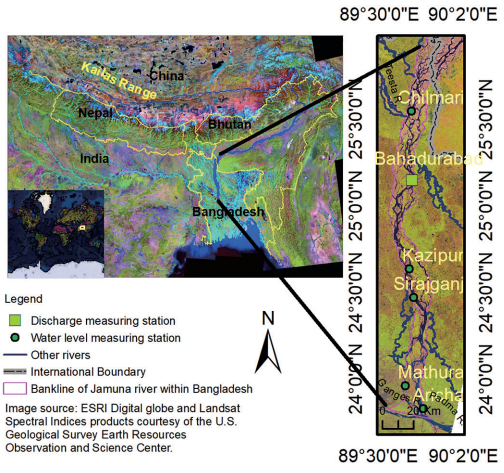

Fig. 1 Map of study area

pared to that of compound bars, which can migrate upstream, downstream, and even laterally by being collated with other bars (Bridge, 1993). Hence the planform changes of the river become very unpredictable due to the dynamic characteristics of these bars. To understand these dynamics, in this study, we developed a two-dimensional morphodynamic model by incorporating the real river bathymetry and boundary conditions for the year 2011 using Delft3D (flow version 4.00.01.000000) software.

Delft3D is a nonlinear physics-based morpho-dynamic model and its flow module can solve shallow water equations (unsteady) in two dimensions (depth-averaged) and three dimensions (Lesser et al., 2004), but for the sake of computational time, we only used it in two dimensions. In the model, the system of equations consists of horizontal momentum, continuity, transport and turbulence closer. It assumes vertical accelerations are very small compared to gravitational ones, therefore, the vertical momentum equation is reduced to the hydrostatic pressure equation (Lesser et al.; 2004). The finite difference method of alternating direction implicit (ADI) was used to solve the difference equations. Here, the turbulence closer model was achieved by applying a constant horizontal eddy viscosity. See Lesser et al. (2004) and Deltares (2009) for a detailed explanation of the Delft 3D model.

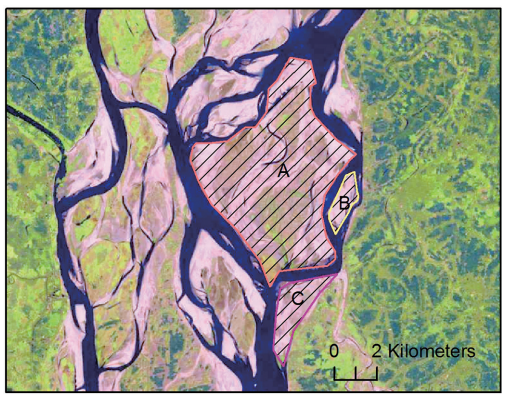

Fig. 2 Examples of different types of bars in Brahmaputra-Jamuna

The simulation was performed for one monsoon period from the 1st of June, 2011 to the 15th of October, 2011. The assumption was that the major morphological changes for that particular year occurred within the peak discharge period of the hydrograph. The model was well calibrated and validated for the year 2012. Then, we calculated some bar scale properties and tried to develop the relationship with the river hydraulics.

In addition, we defined and calculated the migration rate of the compound bars. As the growth of the compound mid-channel bar is not unidirectional; merging of two or three bars during a high flood is very common, we consider the highest lateral distance from the old bar to the newly developed bar in a particular direction as the migration amount/celerity, ω_m of that particular bar for that particular year using Eq. [1]. The analysis was carried out considering every bar as an individual object and it only reflects the annual alteration of the bar shape.

$$\omega_m = \frac{1}{l_{bn}}\left(a_{\max}\right)_{bn} \quad [1]$$

Where

$(a_{\max})_{bn}$=Area of minimum bounding rectangle determined by using Freeman and Shapira (1975), l_{bn}=Longer side length of the minimum bounding rectangle determined by using Freeman and Shapira (1975), $a_{\max}$ is determined by using the following algorithm (Eq. [2] to Eq. [4])

$$a_{\max} = \max_j \left\{a_j\right\} \quad [2]$$

$$\Delta A = \sum_{j=1}^{n} a_j \quad [3]$$

j=number of segments=1, 2,…, n

$$\Delta A = A_f - \sum_{i=1}^{n} A_i \quad [4]$$

Here,

A_f=Area of new compound bar, A_i=Area of old bars from which the compound bar is formed, ΔA=Newly accredited area of that particular compound bar., a_j=Equal width segmented area to the mean flow direction, a_{max}=Area of the largest segment a_j

Fig. 3 shows a simple example of bar migration calculation definitions of a compound bar. Here, b_1,b_2 and b_3 (Fig. 3a) are the old bars from which a new compound bar b_f (Fig. 3b) has been formed. Figs. 3c and d show the definitions of terms used in Eq. [3] and [4].

We validated the migration rate using dry season satellite imagery, Indian Remote Sensing Linear Integrated self-scanning III (IRS-LISS III) images from 2011 to 2012, as described in Section 3. The images represent the dry season scenario as most of the images were captured in February.

2. 2 BAR PROPERTIES

We defined the bar properties following the definitions used by previous researchers, Garcia and Nino (1993), Schuurman et al. (2013) and Eaton and Church (2011). For determining the bar length, one bar was treated as an individual object and the longest axis gave the length of the bar, L and the difference between trough and crest levels gave the value of bar amplitude, H. For dimensional analysis, dimensionless bar height H_b was calculated by dividing the bar amplitude H by the maxi-

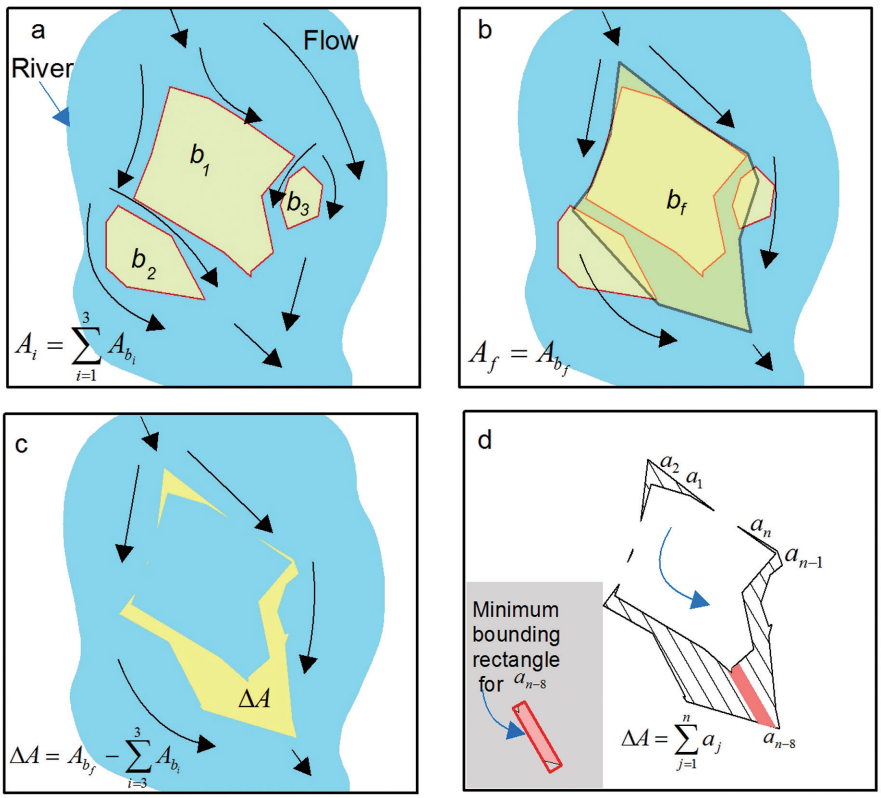

Fig. 3 Schematic definition figure for bar migration calculation

mum scour depth S_0 (S_0 represents the general scour due to fluvial erosion). The constant channel width of the river, W was determined by measuring the width of the bankline of the river of the year 2011 every 10 km and calculating their average. This constant channel width, W was considered for estimating the river's width/depth, β and it is defined by dividing this width by the monthly maximum water depth d within the simulation area. The relative migration rate, ω was defined by the ratio of the migration rate of that particular bar to the monthly mean flow velocity, U_o. Aspect ratio, α is defined by the bar length to the width ratio, $\frac{L}{W}$.

The dimensionless stream power Ω^* was calculated by Eq. [5]

$$\Omega^* = \frac{gdSU_0}{\left[g\Delta D_{50}\right]^{3/2}} \quad [5]$$

Here g is gravitational acceleration, S defines the slope and D_{50} represents the median grain size of the sediment. Δ is the submerged specific gravity of sediment calculated by using the following Eq. [6]

$$\Delta = \frac{\rho_s - \rho_f}{\rho_f} \quad [6]$$

where ρ_s is the density of sand and ρ_f is the density of water.

2. 3 DESCRIPTION OF 2D MORPHODYNAMIC MODEL

A two-dimensional depth average morphodynamic model was developed using Delft3D software (flow version 4.00.01.000000) by applying the following hydrodynamic equations.

Conservation of mass was calculated by using the continuity equation (Eq. [7]):

$$\frac{\partial h}{\partial t} + \frac{\partial (hu)}{\partial x} + \frac{\partial (hv)}{\partial y} = 0 \quad [7]$$

In the x-direction, conservation of momentum (Eq. [8]):

$$\frac{\partial u}{\partial t} + u\frac{\partial u}{\partial x} + v\frac{\partial u}{\partial y} + g\frac{\partial \eta}{\partial x} + \frac{gn^2}{\sqrt[3]{h}}\left(\frac{u(u^2+v^2)}{h}\right) - v_t\left(\frac{\partial^2 u}{\partial x^2} + \frac{\partial^2 u}{\partial y^2}\right) = 0 \quad [8]$$

In the y-direction, conservation of momentum (Eq. [9]):

$$\frac{\partial v}{\partial t} + u\frac{\partial v}{\partial x} + v\frac{\partial v}{\partial y} + g\frac{\partial \eta}{\partial y} + \frac{gn^2}{\sqrt[3]{h}}\left(\frac{v(u^2+v^2)}{h}\right) - v_t\left(\frac{\partial^2 v}{\partial x^2} + \frac{\partial^2 v}{\partial y^2}\right) = 0 \quad [9]$$

Where

η=water level elevation with respect to datum (here in m), h=water depth (m), u,v=depth average velocity in the x and y directions, respectively (m/s), g=acceleration due to gravity (m/s^{-2}), v_t=kinetic eddy viscosity (m^2/s), n=Manning's coefficient (sm$^{-1/3}$)

Kabir and Ahmed (1996) compared different sediment transport formulae using field data (collected by Flood Action Plan -24) and concluded that Van Rijn (1984) estimates the peak period sediment discharge well. Therefore, we also adopted this formula for estimating sediment discharge considering the equilibrium sand concentration at the inflow boundary. The total load, q_θ(Eq. [10]) is calculated using the bed load transport, $q_{\theta b}$ and the suspended-load transport, $q_{\theta s}$:

$$q_\theta = q_{\theta b} + q_{\theta s} \quad [10]$$

The bed load transport rate $q_{\theta b}$ is computed by Eq. [11]

$$q_{\theta b} = \begin{cases} 0.053\sqrt{\Delta g D_{50}^3}\, D_*^{-0.3}\left(\frac{\mu_c\tau - \tau_c}{\tau_c}\right)^{2.1} & if \left(\frac{\mu_c\tau - \tau_c}{\tau_c}\right) < 3.0 \\ 0.1\sqrt{\Delta g D_{50}^3}\, D_*^{-0.3}\left(\frac{\mu_c\tau - \tau_c}{\tau_c}\right)^{1.5} & if \left(\frac{\mu_c\tau - \tau_c}{\tau_c}\right) \geq 3.0 \end{cases} \quad [11]$$

The suspended-load transport $q_{\theta s}$ is defined by Eq. [12]

$$q_{\theta S} = f_s UhC_a \quad [12]$$

Where, τ_c=critical bed shear stress and τ=bed shear stress, μ_c is the ratio between the total bed roughness and the grain related bed roughness and U is the depth-averaged flow velocity in the flow direction. The dimensionless particle parameter is D^* defined by Eq. [13]

$$D^* = D_{50}\left(\frac{(s-1)g}{\vartheta^2}\right)^{1/3} \quad [13]$$

Here, s is the specific density (ρ_s/ρ_f), ϑ is the kinematic viscosity coefficient

f_s=the shape factor for the vertical distribution of suspended sediment and is determined by Eq. [14]

$$f_s = \frac{\left(\frac{a}{h}\right)^{z'} - \left(\frac{a}{h}\right)^{1.2}}{\left(1-\frac{a}{h}\right)^{z'}\left(1.2-z'\right)} \quad [14]$$

Here, a=Van Rijn's reference height and is determined by Eq [15].

$$a = \min\left[\max\{f_a.k_s, \frac{\Delta_r}{2}, 0.01h\}, 0.20h\right] \quad [15]$$

$$Z' = Z + \varphi \quad [16]$$

Z is the suspension parameter and is determined by Eq. [17] and φ is the overall correction factor.

$$Z = \frac{\omega_s}{\psi\kappa u_*} \quad [17]$$

Here ω_s is the particle fall velocity of suspended sediment, Ψ is the coefficient related to the diffusion of sediment particles, κ is the constant of Von-Karman and u_* is the overall bed share velocity.

f_a=Van Rijn's reference height proportionality factor

k_s=Current related effective roughness height

C_a=reference concentration (VanRijn, 1984) and is determined by Eq. [18]

$$C_a = 0.015\rho_s \frac{D_{50}T^{1.5}}{aD_*^{0.3}} \quad [18]$$

Here, T is the nondimensional bed share stress and is determined using VanRijn (1984).

The bed slope effect was considered and directional sediment transport derivatives q_x and q_y were calculated by using the following equations (Eq. [19] and Eq. [20]).

$$q_x = q_b(\cos\varphi_\tau - f(\theta)\frac{\partial\eta_b}{\partial x}) \quad [19]$$

$$q_y = q_b(\sin\varphi_\tau - f(\theta)\frac{\partial\eta_b}{\partial y}) \quad [20]$$

$$f(\theta) = \frac{1}{\varepsilon\theta^\gamma} \quad [21]$$

θ is the shield mobility parameter, η_b is the bed level ε, γ is the calibration parameter and φ_τ is the angle between the downstream direction (x-axis) and the sediment transport vector, and modification is made by the spiral flow using Eq. [22]

$$\tan\varphi_t = \frac{v}{u} - \frac{2}{\kappa^2}\left(1 - \frac{n\sqrt{g}}{\kappa h^{1/6}}\right)\frac{h}{R} \quad [22]$$

R=radius of local streamline curvature

$\partial\eta_b$ is the change in bed level and it is calculated by using the Exner (1925) equation for conservation of mass for sediment calculated following Eq. [23]

$$\partial\eta_b \Big/ \partial t = MF\left(\frac{\Delta q_x}{\Delta x} + \frac{\Delta q_y}{\Delta y}\right) \quad [23]$$

Here, MF is the morphological acceleration factor to reduce the computational time step to adapt the morphology.

2. 3. 1 MODEL SCHEMATIZATION

For the numerical model, a 225-km long curvilinear grid was constructed with an average width of 13 km; starting from almost 10 km downstream of the Noonkhawa water level measuring station

and ending near Aricha (**Fig. 4**). The reach was discretized by 1117x73 grid cells. This grid resolution was chosen to cover every bar by at least two grid cells (grid cell size 201x178 m^2) because the bar size ranges from 549.83x205 m^2 to 28635x10475 m^2 within study reach of Brahmaputra-Jamuna.

The measured river cross-section by the Bangladesh Water Development Board (BWDB) in 2011 was used as the bathymetry data Along with this, for bar-top topography, Shuttle Radar Topography Mission (SRTM) data was used in some places.

The simulation period of our model was the 1st of June, 2011 to the 15th of October, 2011 and the boundary conditions are shown in **Fig. 5**. As the upstream boundary condition discharge data was used. The river Brahmaputra-Jamuna has only one discharge measuring station at Bahadurabad (**Fig. 4**), which is situated almost at the middle part of the study reach, and one major contributing tributary, Teesta, also lies within the upper part of the study reach (**Fig 1**). Hence, for estimating the discharge at the upstream boundary, a 1D model was used and the model was calibrated to the flow

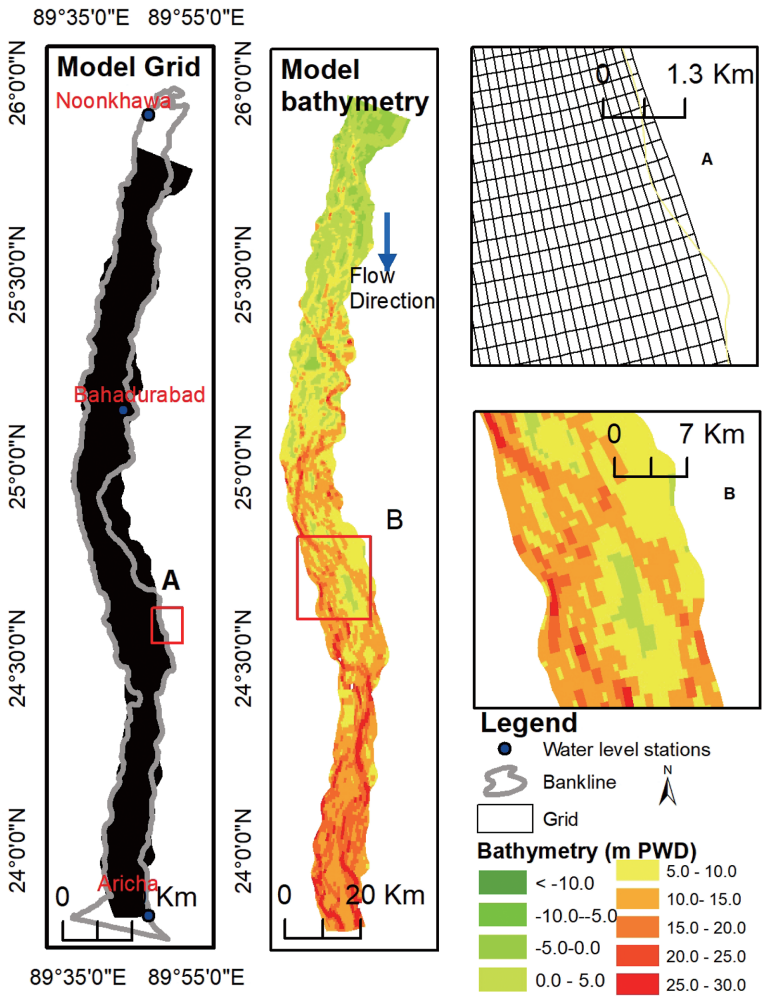

Fig. 4 The model domain

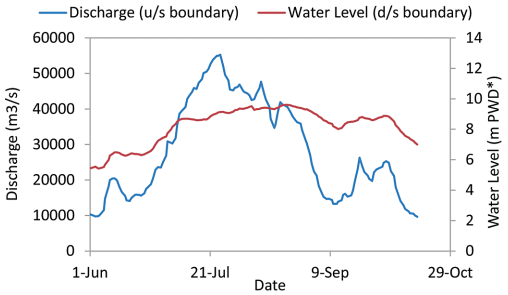

Fig. 5 Boundary conditions of the model

data at Bahadurabad. As the discharge data for Teesta, daily average time series data was used. As the downstream boundary, the water level data of Aricha of the year 2011 was used. The water level was measured with respect to Public Works Datum (PWD), which is widely used datum in Bangladesh. It represents 0.46 m below the Mean Sea Level (MSL) datum. The other parameters used in the model are described in Table 1.

As the initial condition, the space varying water level, which confirms the minimum water depth in all channels, was given. The equilibrium sand concentration (VanRijn, 1984) was considered at the inflow boundary for sediment calculation. The initial sediment layer thickness was assumed to be 5 m at the bed. The minimum depth for sediment calculation was considered to be 0.1 m. The morphological acceleration factor (MF) ranges from 1 to 500 (Jang and Shimizu; 2005, Crosato et al., 2011, 2012, Roelvink; 2006 Van der Wegen and Roelvink; 2008 and Lesser et al., 2004). However, we chose the MF value for a braided river and finalized it through trial and error to best match with the real river planform and bathymetry.

2. 3. 2 MODEL CALIBRATION AND VALIDATION

The water level calibration was performed along four points Chilmari, Kazipur, Sirajganj and Mathura respectively while the discharge and sediment calibration were performed only for Bahadurabad station (Locations are shown in Fig. 1). Figs. 6a and 6b show the discharge, water level calibration results of the model at Bahadurabad and Mathura, respectively. The calibration of sediment was performed using the data set of sediment from 1968 to 2001 measured by BWDB and by the Flood Action Plan-24 (FAP-24) study due to the lack of recent data, which is shown in Fig. 6c. In FAP-24 study, sediment data represents the river conditions for a particular period (mainly the year 1993). For this reason, some discrepancies are found in this dataset. As mentioned earlier, using the equilibrium sediment concentration profile at the inflow boundary and using the Van Rijn sediment transport formula we calculated the sediment load at Bahadurabad. A comparison between the calculated and the observed sediment load is shown in Fig. 6c.

A verification of the model for the water level at Sirajganj is shown in Fig. 6d. In this study, the model was verified for the hydraulic conditions of the year 2012.

Table 1 Boundary Conditions and Model Parameters

PARAMETER	UNIT	BASE CONDITION
MEDIAN GRAIN SIZE, D_{50}	μm	277
DENSITY OF SEDIMENT, ρ_s	kg/m^3	2650
DENSITY OF WATER ρ_f	kg/m^3	1000
SUBMERGED SPECIFIC DENSITY OF SEDIMENT, Δ	–	1.65
VAN RIJN'S REFERENCE HEIGHT FACTOR, f_a	–	2
HORIZONTAL EDDY VISCOSITY	m^{2}s^{-1}	1
HYDRODYNAMIC TIME STEP	s	48
MORPHO-DYNAMIC TIME STEP	s	144
GRID CELL DIMENSION	m^2	201*178
ROUGHNESS (MANNING'S)	s/[m$^{1/3}$]	0.027
MORPHOLOGICAL ACCELERATION FACTOR, *MF*	–	3
CALIBRATION PARAMETER ε	–	0.70
CALIBRATION PARAMETER γ	–	0.5
THRESHOLD SEDIMENT THICKNESS	m	0.005

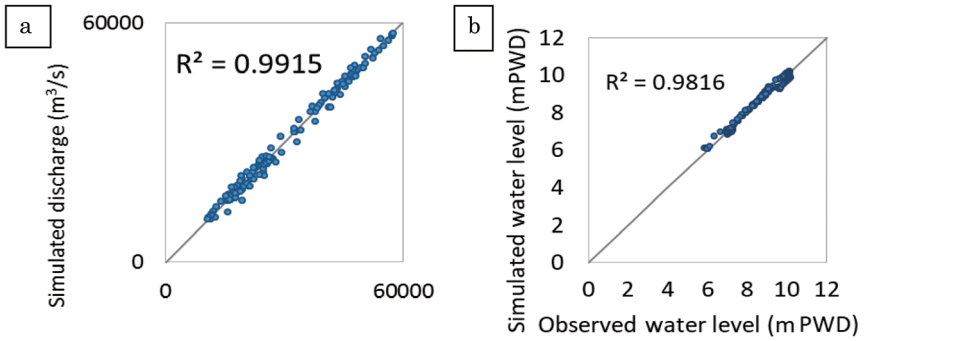

a) Comparison between simulated and observed water level at Mathura

b) Comparison between simulated and observed discharge at Bahadurabad

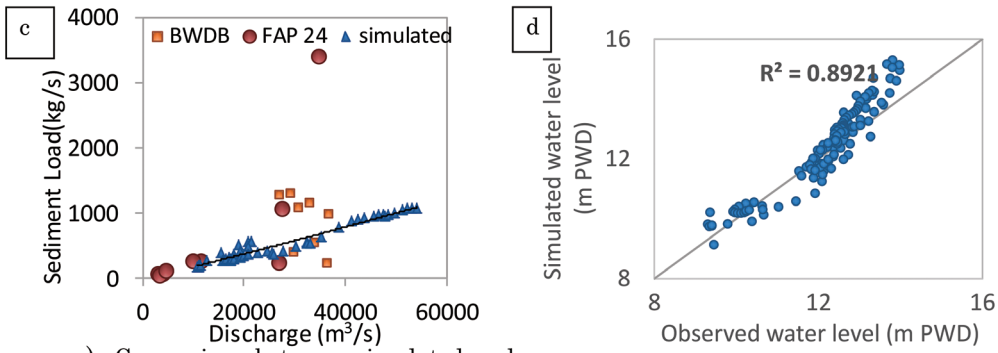

c) Comparison between simulated and observed sediment load at Bahadurabad

d) Comparison between simulated and observed water level at Sirajganj

Fig. 6 Calibration of the model for the hydraulic conditions of the year 2011 (a,b and c) and validation of the model for the hydraulic conditions of the year 2012 (d)

3. RESULTS

3.1 OVERALL PLANFORM, BED LEVEL AND BAR MIGRATION RATE OF THE RIVER

The planform from the satellite image and the simulated planform are shown in Figs. 7a and b, respectively. The model can predict the main anabranch but in the case of small-scale morphology, there are some discrepancies. For example the model did not predict the alignment of chute channels well (Figs. 7 c and d).

As the model was simulated only for one peak season, no huge bed level changes were observed except in some confluences, where a huge scour (like 23.66 m PWD in Sirajganj) was observed (Fig. 7b). Fig. 8 shows an example of the cross-sectional change of the river during the simulation period (the cross-section was taken along the Bahadurabad discharge measuring station). This figure indicates that a major change occurred within 2.5 months as the peak discharge occurred during this time. During this period, the average of net river bed change was -0.22 m (erosion) along this section. After that, the average of net change was aggradation (0.02 m) along this section.

Fig. 9 shows a histogram of the bed level

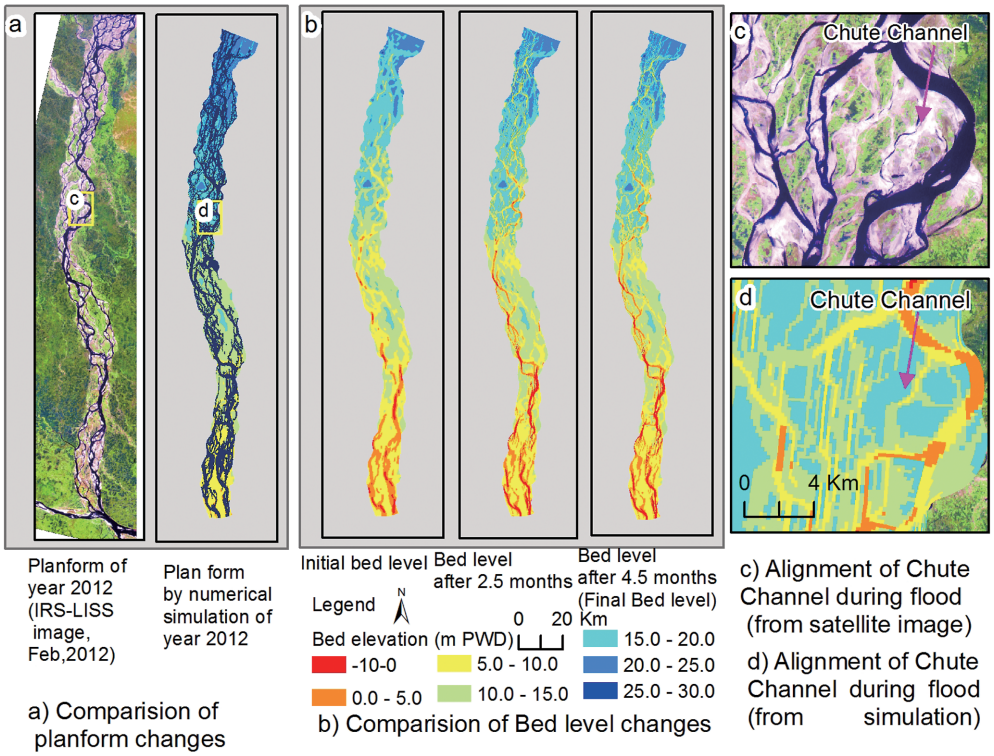

Fig. 7 Comparison of real and simulated planform and time series bed level changes

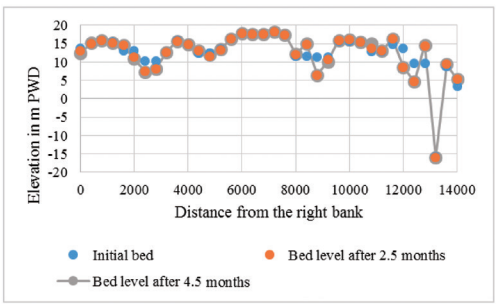

Fig. 8 Bed level at different time along the cross-section of Bahaduraba discharge measuring station

change by calculation of the model results. The bed level change data shows a bimodal distribution as it represents the distribution of two processes (erosion and deposition) combined into one dataset. This figure indicates that the maximum frequency of deposition is from 0 to 1 m. But the maximum frequency is from 4 m to 5 m for erosion.

An example of bar migration is shown in Fig. 10. Here, the black line shows the area of the bar in 2011 and the starting of the simulation and the red line shows the area of the bar in 2012 or the end of the simulation. The satellite image analysis indicates that the migration rate was 1.18 km while the simulation results indicate that the migration rate was 1.10 km for that particular bar.

For the overall calculation of the bar migration rate, all bars (over 300 bars) were considered. Fig. 11 shows a comparison of the bar migration rate derived from satellite images and simulation. This figure indicates that the prediction of the spatial bar growth by simulation is comparable to the actual one. Both the simulation results and satellite imagery analysis show the migration rate of the bar recedes with the growth of the bar. A

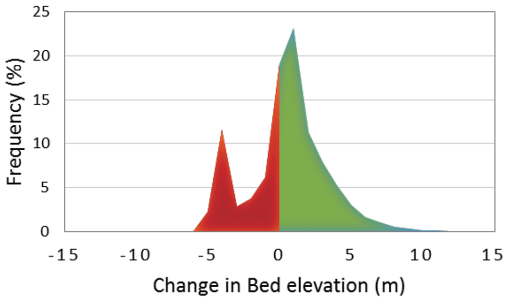

Fig. 9 Histogram of bed level changes

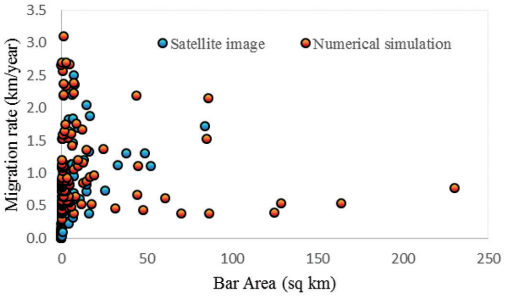

Fig. 11 Comparison of bar migration rate derived from satellite image analysis and numerical simulation

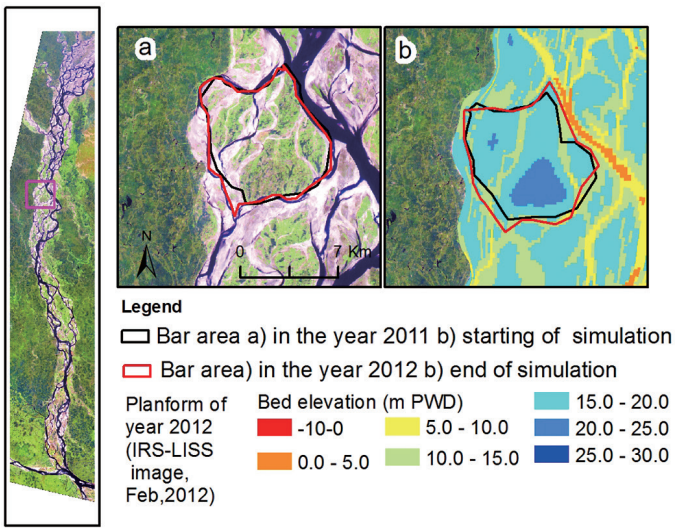

Fig. 10. Map showing an example of bar migration of one bar.

higher migration rate was observed when the bar area was less than 25 km^2. This rate is very high (3 or 2.5 km/year) when the bar area is less than 6 km^2 but after that, it becomes 1.5 to 1 km/year. The average migration rate of bars is 1.05 km/year (standard deviation is 0.65 km/year) but satellite image analysis shows this rate was 0.04 km/year (standard deviation is 0.21 km/year). In the case of estimating the migration rate from satellite images, the images represent the situation for the dry period. The bars may experience erosion during the end of the monsoon to the dry period, especially the small bars. But in the case of simulation, the migration rate was measured just after the monsoon season. Another reason for this discrepancy is the selection of the MF value. As mentioned earlier, this value has a very wide range, and bed level adaptation and morphological changes depend on it.

3.2 BAR PROPERTIES

Here, bar properties were analyzed considering monthly changes. From the simulation results, the dimensionless bar height and bar length are

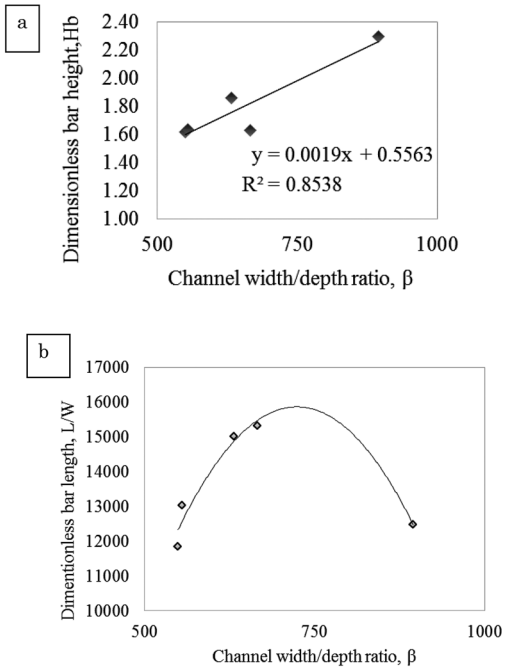

Fig. 12 Relation between dimensionless width-depth ratio to a) dimensionless bar height b) dimensionless bar length

plotted in Figs. 12 a and b (the data represents the monthly data). The results of the dimensionless bar height, H_b analysis indicates a good linear correlation with width/depth ratio, β.

But the dimensionless bar length shows a nonlinear relationship with β and it seems there is a critical value of L/W (here it is around 15000) beyond which the bar does not elongate laterally (Fig. 12b). But the linear theory of bar indicates no such phenomenon for a straight channel and meandering channels and according to this theory, this value increases with the increment of β.

Figs. 13a, b and c show the relationship among the dimensionless migration speed of the bar as the function width/depth ratio β, bar aspect ratio, α and the dimensionless stream power, Ω^* (the data represents the monthly propagation). Fig. 13a indicates that with the increase of width/depth ratio$\beta$from 549 to 665 the dimensionless

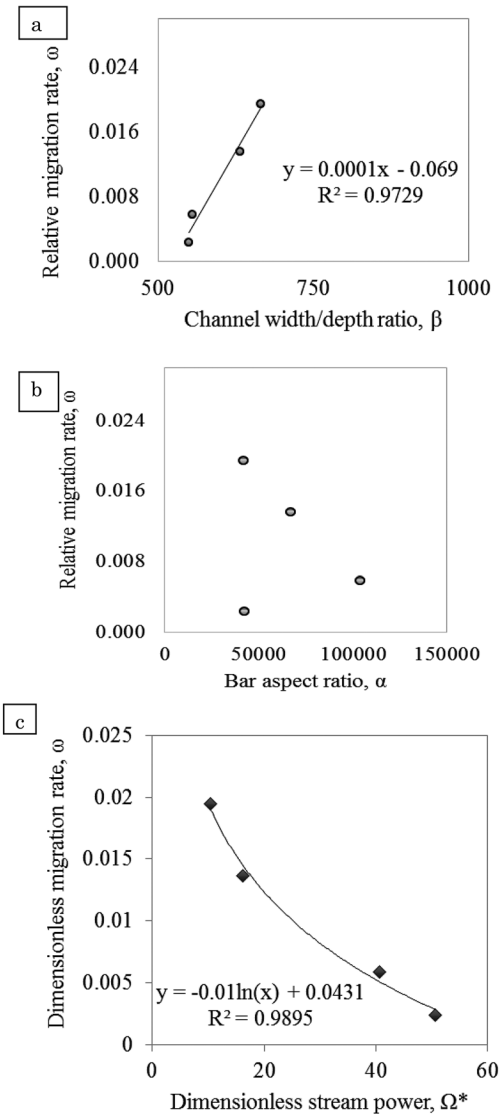

Fig. 13 Relationship between dimensionless migration speed to a) width-depth ratio b) bar aspect ratio and c) channel speed stream power

migration rate also increases from 0.0024 to 0.019. Fig. 13b reveals that the dimensionless migration rate is higher (0.019) for a relatively low aspect ratio bar. Fig. 13c indicates that with the increase of dimensionless stream power Ω^*, the dimensionless migration decrease maintains a nonlinear relationship.

4. DISCUSSION

In this paper, several phenomena of a braided bar are investigated using numerical simulations.

Doeschl et al. (2009) and Ashmore (2013) show the change of bed elevation of another braided river using a physics-based model, laboratory experiment, and field data and summarize a similar type of distribution, which we obtained in the bed elevation change histogram shown in Fig. 9.

The rate of migration seems to be higher compared with that in previous researches; Bridge (1993) estimates this rate is 500 m per year. But they consider only one mid-channel bar in Brahmaputra-Jamuna for their analysis.

The dimensionless analysis indicates that the bar height of a braided bar behaves similarly to bars in straight channels or meandering ones as shown by Garcia and Nino (1993), but it shows a critical point in the case of dimensionless bar length. This analysis indicates there may also exist a suppression point for a braided bar in terms of the $\frac{L}{W}$ ratio.

These simulation results also indicate that the bars in the upper part of the river experience a lower average depth (Fig. 7). This part also shows higher braiding intensity (Sarker et al., 2003; ISPAN, 1993). Sarker et al. (2003). Egozi and Ashmore (2008); Bertoldi et al. (2009) and Sarker et al. (2014) showed that the braiding intensity increases with the increase of discharge both for gravel-bed and sand-bed braided rivers and our results of dimensionless migration rate and stream power analysis also indicate that higher stream power is less favorable for the spatial growth of a bar. Therefore, in the case of bars with a relatively higher spatial area, the bar splitting process governs rather than the migration process.

5. CONCLUSION

Based on our simulations and analysis, we concluded the following:

- The complex growth of a compound bar can be predicted using a 2D morpho-dynamic model. But finer bathymetry data is needed to simulate some small-scale properties (e.g. formation of chute channel over the bar).
- The frequency of deposition on a river bed or a braided plain was higher compared to the erosion due to the response of unsteady discharge and water level change in the study reach of Brahmaputra-Jamuna for that particular year.
- A dimensionless bar height behaves similar to a straight or meandering river but the dimensionless bar length behaves differently. The dimensionless bar property analysis indicates that the spatial growth of a braided bar can be skillfully controlled by controlling the width–depth ratio and channel discharge.
- The migration rate of a bar naturally recedes with its growth. Hence, this phenomenon can also be used for better management of a braided river.

ACKNOWLEDGMENTS

The authors are grateful for the JST-JICA funded SATREPS project "Research on Disaster Prevention/Mitigation Measures against Floods and Storm Surges in Bangladesh" for funding this research. The authors express their thanks to Bangladesh Water Development Board (BWDB), Center for Environmental and Geographic Information Services (CEGIS) and Prof. Dr. Mostafa Ali of Bangladesh University of Engineering and Technology (BUET) for their immense support in data collection.

REFERENCES

Ashmore, P.: Morphology and dynamics of braided rivers. In: Shroder, J. (Editor in Chief), Wohl, E. (Ed.), Treatise on Geomorphology. Academic

Press, San Diego, CA, Vol.9, Fluvial Geomorphology, pp.289–312, 2013.

Ashworth, J.P., G.H. Sambrook Smith, J.L. Best, J.S. Bridge, S.N. Lane, I.A. Lunt, A.J.H. Reesink, C.J. Simpson, and R.E. Thomas: Evolution and sedimentology of a channel fill in the sandy braided South Saskatchewan River and its comparison to the deposits of an adjacent compound bar. Sedimentology, Vol.58 (7), pp.1860–1883, 2011.

Baki, A. B. M., and Gan, T. Y.: Riverbank migration and island dynamics of the braided Jamuna River of the Ganges-Brahmaputra basin using multi-temporal Landsat images. Quaternary International, Vol.263, pp.148–161, 2012.

Bertoldi, W., Zanoni, L., and Tubino, M.: Planform dynamics of braided streams. Earth Surface Processes and Landforms, Vol.34(4), pp.547–557, 2009.

Blondeaux, P., and Seminara, G: A unified bar bend theory of river meanders. J. Fluid Mech., Vol.157, pp.449–470, 1987. doi:10.1017/S0022112085002440

Bridge, J.S.: The interaction between channel geometry, water flow, sediment transport and deposition in braided rivers. In: Braided Rivers (Eds Best, J.L., and Bristow, C.S.), Special Publication of the Geological Society of London, No.75, London, 13–71, 1993.

Crosato, A., E. Mosselman, F. B. Desta, and W. S. J. Uijttewaal: Experimental and numerical evidence for intrinsic nonmigrating bars in alluvial channels. Water Resour. Res., 47, W03511, 2011. doi:10.1029/2010WR009714.

Crosato, A., F. B. Desta, J. Cornelisse, F. Schuurman, and W. S. J. Uijttewaal: Experimental and numerical findings on the long-term evolution of migrating alternate bars in alluvial channels. Water Resour. Res.,48, W06524, 2012. doi:10.1029/2011WR011320.

Colombini, M., Seminara, G. and Tubino, M.: Finite–amplitude alternate bars. J. Fluid Mech., Vol.181, pp.213–232, 1987.

Deltares: Delft3D-FLOW User Manual: Simulation of Multi–Dimensional Hydrodynamic Flows and Transport Phenomena, Including Sediments, Deltares, Delft, The Netherlands, p.630, 2009.

Doeschl, A. B., Ashmore, P. E., and Davison, M. A. T. T.: Methods for assessing exploratory computational models of braided rivers. Braided Rivers: Process, Deposits, Ecology and Management, International Association of Sedimentologists Special Publication, 36, pp.177–197, 2009.

Eaton, B. C., and Church, M.: A rational sediment transport scaling relation based on dimensionless stream power. Earth Surface Processes and Landforms, Vol.36(7), pp.901–910, 2011.

Egozi R, Ashmore P.: Experimental analysis of braided channel pattern response to increased discharge. Journal of Geophysical Research, Vol., 114: pp.1–15, 2009.

Exner, F.M. On the interaction between water and sediment in rivers. Akad. Wiss. Wien Math. Naturwiss. Klasse, Vol. 134(2a), pp.165–204, 1925.

Freeman, H., and Shapira, R.: Determining the minimum-area encasing rectangle for an arbitrary closed curve. Communications of the ACM, Vol.18 (7), pp.409–413, 1975.

Flood Action Plan 24: River Survey Project, Final Report, Main Volume (prepared for FPCO), Dhaka, Bangladesh, p.280,. 1996.

Garcia, M. and Nino, Y.: Dynamics of sediment bars in straight and meandering channels: experiments on the resonance phenomenon. J. Hydr. Res., Vol. 31(6), pp.739–761, 1993.

Ikeda, S.: Experiments by Engels on alternate bars. Summer School on Stability of River and Coastal Forms, La Colombella, Perugia, Italy, 3–14 Sept. 1990.

ISPAN (FAP 16 and FAP 19): The Dynamic Physical and Human Environment of Riverine Charlands: Jamuna, Dhaka, Bangladesh, 1993.

Jang, C. L., and Shimizu, Y.: Numerical simulation of relatively wide, shallow channels with erodible banks. J. Hydraul. Eng., 131(7), pp.565–575, 2005. doi:10.1061/(ASCE)0733–9429(2005)131: 7 (565).

Kabir, M. R., and Ahmed, N.: Bed shear stress for sediment transportation in the River Jamuna. Journal of Civil Engineering, The Institution of Engineers, Bangladesh CE24, 5568. 1996.

Kleinhans, M. G. and van den Berg, J. H.: River channel and bar patterns explained and predicted by an empirical and a physics–based method. Earth Surf. Process. Landforms, Vol.36, pp.721–738, 2011, doi:10.1002/esp.2090

Lesser, G. R., Roelvink, J. A., Van Kester, J. A. T. M., and Stelling, G. S.: Development and validation of a three-dimensional morphological model. Coastal Engineering, Vol.51 (8), pp.883-915, 2004.

Muramoto, Y. and Y. Fujita, A.: Classification and formative conditions of river bed configuration of meso scale. Proc. 22nd Japanese Conf. on Hydraulics, Japan Soc. Civ. Eng., pp.275-282, 1978.

Roelvink, J. A.: Coastal morphodynamic evolution techniques. Coastal Eng., 53(2-3), pp.277-287, 2006. doi:10.1016/j.coastaleng.2005. 10.015

Sarker, M.H., Haque, I., Alam, M. and Koudstaal, R., Rivers, chars and char dwellers of Bangladesh. International Journal River Basin Management, Vol. 1, pp.61-80, 2003.

Sarker, M. H., Thorne, C. R., Aktar, M. N., and Ferdous, M. R.: Morpho-dynamics of the Brahmaputra-Jamuna River. Bangladesh. Geomorphology, Vol.215, pp.45-59, 2014.

Schuurman, F., Marra, W. A., and Kleinhans, M. G.: Physics based modeling of large braided sandbed rivers: Bar pattern formation, dynamics, and sensitivity. Journal of Geophysical Research: Earth Surface, Vol.118 (4), pp.2509-2527, 2013.

Van Rijn, L.C. Sediment transport, Part I: Bed load transport. J. Hydraul. Eng., Vol.110(10), pp.1431-1456, 1984. doi:10.1061/(ASCE)07339429(1984)110:10(1431)

Van der Wegen, M., and Roelvink, J.A.: Long-term morphodynamic evolution of a tidal embayment using a two-dimensional, process-based model. J. Geophys. Res., 113, C03016, 2008. doi: 10.1029/2006JF003983.

Yalin, M.S.: River Mechanics. Pergamon Press, Oxford, 1992.

（投 稿 受 理：平成29年４月７日
訂正稿受理：平成29年７月13日）

要　旨

数多くの川と砂州が同時に変化し影響し合うことによって動的な複雑なネットワークが形成される。本研究で，著者は非定常流よる網状流路の反応特性の調査を行った。特に砂州の動的変化に着目し，ブラマプトラ・ジャムナ川の大部分を占める複合砂州を対象とした数値計算を行った。本研究で，流れの境界条件の非定常性により，研究領域の河床において浸食よりも堆積の方がより多く起こっていることが判明した。また網状流路における砂州の発達過程は蛇行河川と比較して全く異なることが分かった。砂州の空間的広がりは，ある程度流路の流路幅と水深の比によって変わるように見受けられる。そしてその砂州の空間的広がりに伴って，砂州の移動する割合は減少することが分かった。